HHS Public Access

Author manuscript

Cancer Immunol Res. Author manuscript; available in PMC 2019 November 04.

Published in final edited form as:

Cancer Immunol Res. 2019 February ; 7(2): 306–320. doi:10.1158/2326-6066.CIR-18-0310.

Autocrine TGFβ is a Survival Factor for Monocytes and Drives Immunosuppressive Lineage Commitment

Alba Gonzalez-Junca[1,2], **Kyla E. Driscoll**[3], **Ilenia Pellicciotta**[4], **Shisuo Du**[4], **Chen Hao Lo**[4,5], **Ritu Roy**[2,6], **Renate Parry**[7], **Iliana Tenvooren**[8], **Diana M. Marquez**[8], **Matthew H. Spitzer**[2,8], **Mary Helen Barcellos-Hoff**[1,2,*]

[1.]Department of Radiation Oncology, University of California San Francisco, San Francisco, CA 94143, USA

[2.]Helen Diller Family Comprehensive Cancer Center, University of California San Francisco, San Francisco 94158 USA

[3.]TGFβ and Tumor Microenvironment, Eli Lilly and Company, New York, NY 10016, USA

[4.]Department of Radiation Oncology, New York University School of Medicine, New York, NY 10016, USA

[5.]Department of Tumor Biology, Moffitt Cancer Center, Tampa, FL 33612, USA

[6.]Computational Biology and Informatics (CBI), University of California San Francisco, San Francisco, CA 94158, USA

[7.]Varian Medical Systems, Inc., Palo Alto, CA 94304, USA

[8.]Parker Institute for Cancer Immunotherapy, Department of Otolaryngology-Head and Neck Surgery, Department of Microbiology and Immunology, UCSF School of Medicine, San Francisco, CA 94141, USA

Abstract

Transforming growth factor β (TGFβ) is an effector of immune suppression and contributes to a permissive tumor microenvironment that compromises effective immunotherapy. We identified a correlation between *TGFB1* and genes expressed by myeloid cells, but not granulocytes, in TCGA lung adenocarcinoma data, in which high *TGFB1* expression was associated with poor survival. To determine whether TGFβ affected cell fate decisions and lineage commitment, we studied primary cultures of $CD14^+$ monocytes isolated from peripheral blood of healthy donors. We discovered that TGFβ was a survival factor for $CD14^+$ monocytes, which rapidly executed an apoptotic program in its absence. Continued exposure to TGFβ in combination with granulocyte-macrophage colony stimulating factor (GM-CSF) and interleukin 6 (IL6) amplified HLA-

[*]Corresponding author: Department of Radiation Oncology, University of California, San Francisco; 2340 Sutter Street, San Francisco, CA 94143, MaryHelen.Barcellos-Hoff@ucsf.edu, Telephone: (+1) 415-476-8193.

Authorship contributions

Alba Gonzalez-Junca designed and executed experiments, analyzed results and contributed to writing the manuscript. Kyla E Driscoll and Ilenia Pellicciotta contributed to experiment design and manuscript preparation. Shisuo Du and Roger Lo performed the staining and analysis of the lung TMA. Ritu Roy contributed to bioinformatics data analysis. Renate Parry revised the manuscript. Iliana Tenvooren, Diana Marquez and Matthew Spitzer performed and analyzed the CyTOF experiment. Mary Helen Barcellos-Hoff supervised experimental design and prepared the manuscript.

$DR^{low}CD14^{+}CD11b^{+}CD33^{+}$ myeloid derived suppressor cells (MDSCs) at the expense of macrophage and dendritic cell (DC) differentiation. MDSCs generated in the presence of TGFβ were more effective in suppressing T-cell proliferation and promoted the T regulatory cell phenotype. In contrast, inhibition of TGFβ signaling using a small molecule inhibitor of receptor kinase activity in $CD14^{+}$ monocytes treated with GM-CSF and IL6 decreased MDSC differentiation and increased differentiation to pro-inflammatory macrophages and antigen-presenting DCs. The effect of autocrine and paracrine TGFβ on myeloid cell survival and lineage commitment suggests that pharmacological inhibition of TGFβ-dependent signaling in cancer would favor antitumor immunity.

Keywords

TGFβ; innate immunity; immunosuppression; myeloid-derived suppressive cells; monocyte lineage commitment

Introduction

The pleiotropic cytokine transforming growth factor β (TGFβ) is regulated under physiological conditions, for which it has roles in development, wound healing, and tissue homeostasis (1). *TGFB1* encodes a polypeptide that forms a secreted complex consisting of latency-associated peptide noncovalently associated with TGFβ. Latent TGFβ is sequestered in the extracellular matrix and must be activated to release TGFβ to bind the ubiquitous type I and II receptors that initiate signaling, which in turn causes nuclear localization of phosphorylated SMAD 2/3 (pSMAD). In cancer, malignant cells can activate abundant TGFβ, which also regulates the tumor microenvironment (TME) (1,2) and mediates the response to cytotoxic therapy (3). TGFβ is implicated in failure to respond to immunotherapy (4–6), and it is thought to stimulate monocyte chemotaxis (7), promote immunosuppressive cell types, including regulatory T cells (Tregs) and macrophages, and suppresses T-cell proliferation (1). TGFβ activation is also associated with activated immune cells, raising the potential for positive reinforcement of immunosuppression.

Myeloid-derived suppressor cells (MDSCs) are a heterogeneous population that functionally limits antitumor immunity (8,9). MDSCs are defined by their suppression of T-cell proliferation (10). In humans, MDSCs can be subdivided into monocytic MDSCs, which are characterized by the expression of markers that include CD14, CD33 (Siglec-3), and CD11b and by the lack of the lineage differentiation marker HLA-DR, whereas granulocytic MDSCs display CD15 and dim CD33 staining (11). MDSCs suppress cytotoxic T-cell activation and proliferation by several mechanisms, including depleting arginine through the expression of arginase-1, increasing nitric oxide, and by activating TGFβ (12). MDSCs can also promote differentiation of naïve T cells to an immunosuppressive Treg phenotype. MDSCs are reported to suppress immune rejection of cancer, compromise immunotherapy, promote tumor growth, and impede response to cytotoxic therapy (8,11). Patients with abundant MDSCs have lower overall survival and decreased progression-free survival in several cancer types (13).

Under physiological conditions, $CD14^+$ monocytes exit the bone marrow to circulate in the peripheral blood and can be recruited into tissues to differentiate into macrophages and dendritic cells (DCs), particularly at sites of injury, tissue remodeling, and infection. In certain states and diseases, granulocyte-macrophage colony stimulating factor (GM-CSF) and interleukin 6 (IL6) favor MDSC generation (14). Here, we focused on expanding the understanding of the role that TGFβ plays in the accumulation and differentiation of monocytes once they enter the TGFβ-rich TME. We used primary cultures of $CD14^+$ monocytes isolated from human peripheral blood to investigate the contribution of TGFβ to monocyte lineage commitment and MDSC function.

Materials and Methods

The Cancer Genome Atlas (TCGA) data analysis using cBioportal

cBioportal for cancer genomics (15,16) was used to study gene expression on samples from TCGA corresponding to glioblastoma, non-small cell lung adenocarcinoma (NSCLC), squamous cell carcinoma, melanoma, head and neck, pancreatic adenocarcinoma, liver, kidney, ovarian, bladder, and prostate carcinomas. Kaplan Meier survival analysis was performed using cBioportal.

Healthy donor buffy coat

Buffy coats from 30 donors were obtained from New York City Blood Center (NYCBC, Queens, NY) and from the Pacific Blood Center (San Francisco, CA) donations under standard operating conditions, following all applicable FDA regulations. Individual consent was not required as all donors consented to the possibility of research use at the time of donation. No pre-screening based on age, sex or ethnicity was applied. Buffy coats were kept on ice and processed shortly after reception (less than 8 hours) for peripheral blood mononuclear cells (PBMCs) isolation.

$CD14^+$ cell isolation, separation, and culture

$CD14^+$ cells were freshly isolated from healthy donor buffy PBMCs using $CD14^+$ magnetic beads (Miltenyi Biotech, Catalog number 130-050-201) (Supplementary Fig. S1A). The purity of CD14 selection was greater than 95% (Supplementary Fig. S1B). The $CD14^-$ fraction was viably frozen in 95% FBS and 5% DMSO using a temperature gradient and stored for 5 days at −80C. $CD14^+$ monocytes were then cultured in 10% fetal bovine serum-RPMI (complete) media and the indicated cytokines at the following concentrations: GM-CSF (10 ng/mL; Milteny Biotech Cat # 130-095-372), IL6 (10 ng/mL; Miltenyi Biotech Cat # 130-093-929), TGFβ (500 pg/mL; R&D Systems Cat #240-B-002). In some experiments, the TGFβ type I receptor kinase inhibitor (LY2109761, 2 μM) obtained from Eli Lilly under a Material Transfer Agreement, or a pan TGFβ-neutralizing antibody 1D11 (1 μg/mL; R&D Systems Cat #MAB-1835) were added to complete media.

Immunofluorescence

A lung tumor tissue microarray (TMA) was obtained from US Biomax (BC041114). 90 NSCLC cases were used for the analysis. Tumors were fixed in formalin and embedded in paraffin (FFPE) in the histology core facility (NYU and UCSF). 3 μm-thin sections were

blocked with 0.5% casein and incubated with primary antibodies overnight at 4°C. Slides were incubated at room temperature for one hour with fluorescent-conjugated secondary antibodies (Life Technologies), and 4,6-Diamidino-2-phenylindole (DAPI) for nuclear DNA content and mounted with Vectashield (Vector Labs Cat #H-1000) mounting media and stored at 4°C in the dark.

For cell immunofluorescence, $CD14^+$ cells were fixed with 4% paraformaldehyde (PFA) for 20 minutes, blocked with 0.5% casein, and incubated with primary antibodies overnight at 4°C. Slides were incubated at room temperature for one hour with fluorescent-conjugated secondary antibodies (Life Technologies), and DAPI, and mounted with Vectashield mounting media and stored at 4°C in the dark. High-power field images (20x) were acquired within 3 days on a Zeiss Axiovert 135TV fluorescence microscope equipped with Metamorph software (Molecular Devices, Inc.), and fluorescence was quantified by Fiji/ImageJ using in-house macros to measure mean intensity with a user defined region of interest. Antibodies and dilutions are listed in Supplementary Table S1.

RNA sequencing (RNA-seq)

Specimens for RNA-seq were obtained as described in Supplementary Fig. S1A. RNA was extracted and RNAseq was performed at NYU genomics core facility. RNAseq data was analyzed using the Aroma Framework (17) and Bioconductor (18) implemented in R (19). Data was normalized using the weighted trimmed mean of M-values method from edgeR package (20) and mapped to the reference assembly hg38. Treated and untreated samples were compared separately for each time point, excluding genes with less than 10 counts for any sample for that time point. Linear modeling with weights based on mean-variance relationship (21) and with empirical bayes moderation (22) from the Bioconductor limma package (23) were used to determine differentially expressed genes. Q-values, computed from q-value package (24), < 0.05 were considered significant. Gene set enrichment analysis (GSEA; Broad Institute) was done using the romer method (25) from the limma package in R/Bioconductor and the reference gene sets from the molecular signatures database (MSigDB) (26). The p-values were adjusted for multiple testing by controlling the false discovery rate (FDR) using the Benjamini and Hochberg method for each database and time point. Adjusted p-values <= 0.01 were considered significant. Fastq RNA-seq files were deposited at GEO database (GSE96885).

Gene expression

CD14+ cells were treated as described in the figure legends and lysed with RNA lysis buffer (Qiagen), and RNA was extracted following manufacturer's instructions (RNAeasy, QIAGEN). RNA concentration was measured using Nanodrop. 100 to 300 ng of RNA were used to generate cDNA using Life Technologies Suprescript kit. Gene-expression of the following transcripts was assessed by quantitative real-time PCR (qRT-PCR) using SYBR green (Thermo Fisher/Life Technologies Cat #4309155). Expression of genes was measured using SYBR green quantitative real-time PCR (qRT-PCR) normalized by the expression of 2 endogenous house-keeping genes, *GAPDH* and *RPL13,* using the (2^–ΔΔCt) method Results are shown as mean±SEM as arbitrary units (AU) and normalized to the untreated or GM-CSF+IL-6 treated control sample.

Primers were designed using Roche Universal Probe Library Design Center (https://lifescience.roche.com/en_us/brands/universal-probe-library.html#assay-design-centre).

Gene	Forward Primer Sequence (5′ to 3′)	Reverse Primer Sequence (5′ to 3′)	Gene accession number
TGFB1	GCAGAAGTTGGCATGGTAGC	CCCTGGACACCAACTATTGC	NM_000660.6
SMAD7	AGACAACGTGCTCTTTGTTTTG	AGAGACACCGCTTGGGACT	NM_005904.3
SERPINEA1	CCAGCTGACAACAGGAGGAG	CCCATGAGCTCCTTGTACAGAT	NM_000602.4
RUNX1	CTCCCTGAACCACTCCACTG	TGGGGATGGTTGGATCTG	NM_001754.4
SOX4	AGCCGGAGGAGGAGATGT	TTCTCGGGTCATTTCCTAGC	NM_003107.2
TNFSF14	AG CG AAG GTCTCACG AGGT	CGGTCAAGCTGGAGTTGG	NM_003807.4
CASP1	CCAGGACATTAAAATAAGGAAACTGT	CCAAAAACCTTTACAGAAGGATCTC	NM_033292.3
CD36	CCTCCTTGGCCTGATAGAAA	GTTTGTGCTTGAGCCAGGTT	NM_001001548.2
CARD16	GCCAAATTTGCATCACATACA	GTCCTGCACTGCCTGAAGA	NM_001017534.1
CARD17	CAAGATTCTCAAATAGTACTTCCTTCC	GCTGGGCATCTGTGCTTTAT	NM_001007232.1
THBS1	CAATG CCACAGTTCCTG ATG	TGGAGACCAGCCATCGTC	NM_003246.3
VNN1	TCCTGAGGTGTTGCTGAGTG	AGCGTCCGTCAGTTGACAC	NM_004666.2
GADD45G	CAGCCAAAGTCTTGAACGTG	CCTGGATCAGCGTAAAATGG	NM_006705.3
CD274	TATGGTGGTGCCGACTACAA	TGCTTGTCCAGATGACTTCG	NM_014143.3
NOS2	ATTCTGCTGCTTGCTGAGGT	TTCAAGACCAAATTCCACCAG	NM_000625.4
ARG1	GTTTCTCAAGCAGACCAGCC	GCTCAAGTGCAGCAAAGAGA	NM_001244438.1
CYBB	GACAGAGGGGCTGTTCAATG	GCCCATCAACCGCTATCTT	NM_000397.3
CEBPB	CGCTTACCTCGGCTACCA	ACGAGGAGGACGTGGAGAG	NM_001285879.1
STAT3	CCTCTGCCGGAGAAACAG	CTGTCACTGTAGAGCTGATGGAG	NM_139276.2
S100A8	GCCAAGCCTAACCGCTATAA	ATGATGCCCACGGACTTG	NM_001319196.1
S100A9	CTCCCACGAGAAGATGCAC	GAGGCCTGGCTTATGGTG	NM_002965.3
HLA-A	TGCAAAGGCACCTGAATGT	ACAGGTCAGTGTGGGGACA	NM_002116.7
HLA-DR-A	AGCACTGGGAGTTTGATGCT	GGCACACACCACGTTCTCT	M60334.1
HLA-DR-B	ACTGGAACAGCCAGAAGGAC	TGTGTCTGCAGTAGGTGTCCA	A06805.1
B2M	TTCTGGCCTGGAGGCTATC	TCAGGAAATTTGACTTTCCATTC	NM_004048.2
GAPDH	CAGCCTCCAGATCATCAGCA	TGTGGTCATGAGTCCTTCCA	NM_002046.5
RPL13	CAGCGGCTGAAGGAGTACC	GGTGGCCAGTTTCAGTTCTT	NM_000977.3

Cytokine analysis

2×10^6 freshly isolated $CD14^+$ cells were treated with cytokines GM-CSF and IL6 at the specified concentrations in combination with either TGFβ or LY2109761 at the specified concentrations in complete media for 48 hours. Cytokines were measured in undiluted cell-free supernatants using a multiplexed panel of 42 cytokines and chemokines (MILLIPLEX MAP Human Cytokine/Chemokine Panel I Kit HCYTOMAG-60K). All samples were acquired on a Luminex 200 instrument (Millipore)) using manufacturer's instructions and software. Results were normalized by the number of cells counted at the time of collection (viability was determined by trypan blue exclusion on automatic BioRad cell counter).

Cytokine levels are compared to control (GM-CSF+IL-6 treated) cells. TGFβ1 and latency-associated peptide 1 were measured in supernatants, using a multiplex assay based on Mesoscale Discovery (MSD)® electrochemiluminescence-based ELISA (Mesoscale Diagnostics, LLC) as previously published (27). Protein concentration baselines for complete media with or without cytokines (including TGFβ) were subtracted and values were normalized to the number of live cells (determined by trypan blue exclusion using BioRad cell counter) for each condition.

FACS staining

$CD14^+$ cells treated under the conditions described in figure legends were diluted in FACS buffer (PBS + 10% FBS) and stained using a panel of fluorescent labeled antibodies (Supplementary Table S2) for 45 minutes at 4C°. Cells were then washed with FACS buffer and incubated with LIVE/DEAD® Fixable Yellow Dead Cell Stain (Cat. #L-34959 Invitrogen/Life Technologies, now Thermo Fisher) according to the manufacturer's protocol. Stained cells were washed and resuspended in FACS buffer and analyzed immediately in a BD LSRII Cytometer. Appropriate compensation was performed using compensation beads (UltraComp Beads, Cat. #01-2222-42, Invitrogen/Thermo Fisher), and isotype controls (Supplementary Table S2) were run in parallel in each experiment. Data was analyzed using FlowJo v9 and v10 (FlowJo, LLC).

Mass Cytometry (CyTOF)

2×10^6 freshly isolated $CD14^+$ cells were treated with cytokines GM-CSF and IL6 (at the concentrations specified above) in combination with either TGFβ or LY2109761 (at the concentrations indicated above) in complete media for 5 days. Cells were incubated for 1 min with cisplatin (25 μM) to assay nonviable cells resulting in a platinum signal quantifiable by mass cytometry (28). Cells were then fixed with paraformaldehyde and stained with commercially available metal-labeled antibodies (Fluidigm; Supplementary Table S3). Cell populations were analyzed using unsupervised clustering performed using the *clara* algorithm in R and visualized as a force-directed graph in open sourced software Gephi (https://gephi.org/) as previously described (29,30).

Phagocytosis assay

Phagocytic capacity of differentiated myeloid cells was assessed by using a commercially available phagocytosis assay kit IgG-FITC (Cayman, Item № 500290), following manufacturer's instructions. Briefly, $CD14^+$ cells were differentiated for 5 days with GM-CSF+IL6 and with or without the addition of TGFβ or TGFβ inhibitor. Cells were counted, and 10^6 cells were incubated with FITC-IgG latex beads (Item № 500290, Cayman) at 37°C. Cells were then stained with CD45-APC-Cy7, CD11b-Pacific Blue and analyzed by flow cytometry. Alternatively, cells were fixed in 4% PFA on positively charged slides, and stained with anti-CD11b antibody (see Supplementary Table S1) and analyzed using immunofluorescence microscopy. To quantify phagocytosis, the median fluorescence intensity and percent of positive FITC+ cells were quantified on $CD11b^+$ cells using FlowJo (FlowJo, LLC).

Cytotoxic T cell assay

Antigen-presentation capacity of $CD11b^+$ cells was tested by co-culturing with autologous naïve $CD3^+$ T-cells and a human lung cancer cell line, NCI-H1299 (ATCC® CRL-5803). Verified mycoplasma – negative NCI-H1299 cells were purchased from ATCC (Lot number # 58483200) and passaged according to ATCC recommendation less than 6 passages. $CD14^+$ myeloid cells were differentiated for 5 days under the listed conditions, collected, counted and co-cultured at a 1:1 ratio with autologous naïve $CD3^+$ T-cells and adherent H1299. After 48 hr, supernatants containing non-adherent immune cells were discarded, and tumor cells trypsinized for annexin-V flow cytometry.

Statistics

Differences between values measured as a function of treatment of specimens from independent donors (N indicated in figure legends) were analyzed on Prism 7.0 software (GraphPad), using paired t-tests for normal distributions, and Wilcoxon signed rank test for non-parametric variables, unless otherwise indicated. A p value of <0.05 was considered significant.

Results

TGFB1 and myeloid markers are correlated in cancer, including lung adenocarcinoma

To evaluate the relationship between TGFβ and myeloid cells across cancer types, we interrogated The Cancer Genome Atlas (TCGA) samples using cBioportal (15,16). The expression of *TGFB1* was significantly correlated to *ITGAM* (gene encoding for the canonical myeloid marker CD11b) in non-small cell lung adenocarcinoma (NSCLC) samples (Fig. 1A). A similar relationship was observed in glioblastoma, melanoma, colorectal carcinoma, and ovarian cancers (Supplementary Table S4, Supplementary Fig. S2A). *TGFB1* expression was also correlated in NSCLC for myeloid markers *CD14* and *CD33*, which were expressed on monocytic MDSCs (10) but not with granulocyte or neutrophil marker *CEACAM* (CD66b), cross-presenting DC marker *ITGAE* (CD103), or NK marker *NCAM* (CD56) (Fig. 1B).

Due to TGFβ's production as a latent complex, extracellular modification is necessary to release, i.e. activate, TGFβ to bind to ubiquitous receptors. TGFβ receptor activation results in phosphorylation of SMAD (i.e. pSMAD) that is evident in the nucleus. To further assess the relationship between expression of *TGFB1* and myeloid markers, we used antibodies that recognized active TGFβ (after its release from latency associated peptide), pSMAD, and $CD11b^+$ monocytes in NSCLC tissue microarrays. Controls using secondary antibodies alone were negative (Supplementary Fig. S2B). TGFβ immunostaining correlated with nuclear pSMAD intensity, as expected (Supplementary Fig. S2C). TGFβ and pSMAD immunostaining of NSCLC was heterogeneous (Supplementary Fig. S2D). TGFβ activity co-localized with $CD11b^+$ cells in NSCLC (Fig. 1C), and TGFβ staining intensity significantly correlated with frequency of $CD11b^+$ cells (Fig. 1D), which supports a relationship between TGFβ activity and myeloid cells, as was indicated by the TCGA analysis. We found that high *TGFB1* was associated with poor prognosis in lung adenocarcinoma TCGA patients (Fig. 1E, Supplementary Table S5) (31).

TGFβ is a survival factor for myeloid cells

To investigate the effect of TGFβ on myeloid lineage differentiation, we established primary cultures of $CD14^+$ monocytes isolated from the peripheral blood of healthy donors (Supplementary Fig. S1A). The purity of $CD14^+$ cell cultures was greater than 95% (Supplementary Fig. S1B). We noted that the number of viable $CD14^+$ cells in the absence of TGFβ for 24 hours, was less than half that seen in TGFβ-treated cultures (Fig. 2A). The proportion of $CD14^+$ cells significantly decreased in the absence of TGFβ compared to TGFβ treated cultures (Fig. 2B). In contrast, exposure to TGFβ maintained CD14 status and increased cell viability, which resulted in 3-times more $CD14^+$ viable cells after 5 days in culture (Fig. 2C). Thus, TGFβ conferred a specific survival benefit and maintains expression of CD14 on monocytes isolated from PBMCs.

To further explore the consequences of TGFβ in $CD14^+$ monocytes, we used RNA-seq to analyze gene expression at 8, 12, and 36 hours. As expected, gene set enrichment analysis (GSEA) demonstrated enrichment of targets of SMAD2/3 (Supplementary Fig. S3A). TGFβ changed 3,400 genes (q value<0.001) within 8 hours (Fig. 3A). Over 5,000 genes were differentially expressed after 12 hours. The genes regulated in TGFβ-treated monocytes overlapped less than 50% with published gene expression signatures from other myeloid cells and were distinct from that of different myeloid cell populations from Newman et al. (32) (Supplementary Fig. S3B, C). TGFβ induced upregulation of known target genes that included *SMAD7*, *SERPINE1*, *SNAI1, MMP2*, *ADAM12*, *LTBP2*, *PLAU*, *CADH26*, *PDGFA*, and *PDGFB* (Supplementary Table S5). GSEA indicated significant enrichment of published TGFβ signatures and SMAD2/3 regulated genes (33,34), as well as signatures associated with macrophages, cytokines, and hematopoiesis (35,36)(Fig. 3B). TGFβ-regulated transcriptional responses revealed differential expression of myeloid differentiation and survival-related genes (Fig. 3C). Selected genes, validated by qRT-PCR (Fig. 3D), confirmed that TGFβ significantly increased the expression of the transcription factor *RUNX1*, which is known to regulate myeloid cell survival and differentiation (37); *SOX4*, known to prevent p53-mediated apoptosis (38); and *TNFSF14*, which is required for monocyte survival (39). Conversely, TGFβ repressed the expression of *CASP1*, *4*, and *5*, and the caspase-interacting *CARD16* and *CARD17*, responsible for the proteolysis and release of the pro-inflammatory cytokines interleukin 1 beta (IL1β) and IL18, mediators of innate immunity (40).

This RNA-seq analysis suggested that TGFβ suppressed apoptotic programs, which could increase survival of $CD14^+$ monocytes. Accordingly, TGFβ reduced the number of cells positive for annexin V, a surrogate marker of cell death (Fig. 3E) and significantly reduced cleavage of caspase-3, a main effector caspase of the apoptotic cascade (Fig. 3F). GSEA also suggested increased activity of PI3-kinase/AKT signaling, which is a survival pathway for monocytes (41,42). Immunoreactivity of phosphorylated ribosomal protein S6, which is a surrogate for AKT pathway activity, was increased when cells were treated with TGFβ (Fig. 3G). These data indicate that $CD14^+$ monocytes execute an apoptotic program in the absence of TGFβ. Thus, high TGFβ activity in the TME could promote survival of recently recruited $CD14^+$ monocytes.

TGFβ promotes MDSC accumulation at the expense of lineage differentiation

Pathway analysis also suggested that TGFβ influenced differentiation in $CD14^+$ monocytes (Supplementary Fig. S3B), which can differentiate into MDSCs, macrophages, or antigen-presenting DCs, depending on the cytokine composition of the microenvironment. For example, GM-CSF can promote differentiation towards macrophages or DCs (14). The cytokine spectrum of culture supernatants of $CD14^+$ monocytes cultured with GM-CSF and IL6 with or without the addition of TGFβ were analyzed for 42 anti- or pro-inflammatory cytokines and chemokines (Supplementary Fig. S4). Addition of TGFβ to GM-CSF and IL6 significantly reduced the amount of pro-inflammatory and macrophage-secreted cytokines and chemokines, such as chemokine (C-X-C motif) ligand 1 (CXCL1) or growth-regulated oncogene (GRO), monocyte chemoattractant protein 1 and 3 (MCP-1, 3; also known as chemokine (C-C motif) ligand 2 (CCL2)), macrophage inflammatory protein 1 alpha (MIP-1α) also known as chemokine (C-C motif) ligand 3 (CCL3), and transforming growth factor alpha (TGFα). Simultaneously, TGFβ-treated cultures significantly increased the secretion of the anti-inflammatory cytokine interleukin-1 receptor antagonist (IL1Rα) and the Th2-promoting chemokine macrophage-derived cytokine (MDC), also known as chemokine (C-C motif) ligand 22 (CCL22) (Fig. 4A). TGFβ also increased the production of GM-CSF and IL6. Together these results suggest that $CD14^+$ monocytes shifted from a pro-inflammatory phenotype towards a more suppressive cytokine profile when exposed to TGFβ.

A panel of fluorescently labeled antibodies was used to assess the expression of markers typically associated with MDSCs, DCs, and macrophages (gating strategy shown in Supplementary Fig. S5AB). The addition of TGFβ to GM-CSF and IL6 significantly increased the population of $HLADR^{low}CD11b^+CD33^+$ cells (Fig. 4B), indicative of MDSCs (10). Concomitantly, the population of mature DCs expressing the antigen presenting proteins HLA-DR and HLA-1 was significantly reduced after treatment with TGFβ (Fig. 4C). TGFβ addition also reduced the population expressing macrophage marker CD68 (Fig. 4D) and significantly reduced phagocytic capacity, concordant with a decrease in macrophage differentiation (Supplementary Fig. S6A). We further evaluated the gene expression of a panel of immunosuppressive genes (12,14). Expression of *CD274* (PD-L1), *NOS2*, *ARG1*, and *CYBB* (NOX2) was significantly increased when more MDSCs were generated in the presence of TGFβ (Supplementary Fig. S6B). TGFβ also increased the expression of the *CEBP/B* and *STAT3* transcription factors, as well as *S100A8* and *A9* genes, all of which are implicated in the regulation and function of MDSCs (43–45).

MDSCs are defined by their immunosuppressive capacity. To functionally validate MDSCs, $CD11b^+$ cells were sorted from each condition, counted, and co-cultured 1:1 with autologous activated $CD3^+$ T cells (Supplementary Fig. S6C–E). $CD11b^+$ cells generated in the presence of TGFβ were more effective at inhibiting $CD8^+$ T-cell proliferation than cells generated by GM-CSF and IL-6 alone (Fig. 4E). Concordant with decreased proliferation, TGFβ-treated $CD11b^+$ cells also reduced the percentage of $IFN\gamma^+$ cytotoxic T cells (Fig. 4F) and were more proficient in inducing $CD4^+CD25^+FoxP3^+$ Treg conversion (Fig. 4G). To further characterize the cells generated in the absence or presence of TGFβ, we used CyTOF and a panel of 35 myeloid cell phenotypic and functional markers (29). The addition of

TGFβ to GM-CSF and IL6 did not result in a novel population but rather increased the existing population displaying MDSC markers (Supplementary Fig. S7A, B). Collectively, these results indicated that TGFβ promoted MDSC differentiation.

TGFβ promotes MDSC via an autocrine feedback loop

MDSCs are known to activate TGFβ as part of their immunosuppressive repertoire (11). TGFβ frequently regulates its own expression in a positive feedback loop (46). Consistent with this, *TGFB1* expression increased as early as 4 hours after exposure (Fig. 5A). Hence, we asked whether autocrine TGFβ contributed to MDSC generation. To measure TGFβ activity, we analyzed the media conditioned by $CD14^+$ monocytes using a multiplex ELISA that measures active and latent TGFβ1 (27). The amount of active TGFβ1 tripled in short-term (48-hour) cultures (Fig. 5B), whereas the amount of latent TGFβ1 did not change (Fig. 5C), which indicated rapid induction of TGFβ1 activation. In long-term cultures (5 days), $CD14^+$ cells treated with GM-CSF, IL6, and TGFβ produced 5-times as much active TGFβ and almost twice as much latent TGFβ than cultures treated with GMCSF and IL6 alone (Fig. 5D–E). *TGFB1* expression was also increased (Fig. 5F). We then stained cells using antibodies that recognized active TGFβ and pSMAD2, indicative of downstream signaling (Fig. 5G). Both indices significantly increased in monocytes exposed to TGFβ (Fig. 5H–J). These data indicate that TGFβ elicited a feedback loop in monocytes to further amplify its activity.

We noted that GM-CSF and IL6 increased TGFβ activation compared to untreated control. To test whether autocrine TGFβ contributed to the effects of GM-CSF and IL6, we blocked TGFβ signaling using LY2109761, a selective TGFβ type I receptor (TβRI) kinase inhibitor, in combination with GMCSF and IL6 conditioning of $CD14^+$ cells. Treatment with LY2109761 prevented the increase of active TGFβ in the conditioned media (Fig. 5D–E) and resulted in reduced downstream signaling (Fig. 5F–I). We noticed that cells cultured with TGFβ inhibitor for 5 days underwent changed morphology, becoming more adherent and resembling mature macrophages or DCs (Fig. 6A).

Consistent with this, TGFβ signaling blockade increased pro-inflammatory macrophage-derived cytokines present in the supernatants (Fig. 6B, Supplementary Fig. S8), as well as increased type I IFN (IFNα) and IFNγ, which are both implicated in the activation of a Th1 immune response (47). TGFβ inhibition also increased IL2 and other related cytokines, such as IL7 and IL15, which are all implicated in sustaining activation and proliferation of T-cells and NK cells (48). T cell, NK cell, and neutrophil chemoattractant chemokines IL8 (CXCL8), IP-10 (CXCL10), MIP1α, and MIP1β (49) were also significantly increased in $CD14^+$ cell cultures after LY2109761 treatment. At the same time, the immunosuppressive cytokines IL1Rα and CCL22 were significantly reduced when TGFβ was inhibited.

Either inhibition of TGFβ signaling by LY2109761 or ligand blockade using the TGFβ-neutralizing antibody 1D11 produced significantly fewer MDSCs in both total number and percentage (Fig. 6C), whereas the proportion of $CD68^+$ macrophages significantly increased (Fig. 6D). Consistent with an increase in functional macrophages, the phagocytic capacity of cells in these cultures was significantly enhanced (Fig. 6E). $CD68^+$ macrophages expressing M1 marker CD80 were significantly increased, whereas the percentage of $CD163^+$ M2

macrophages significantly decreased upon TGFβ inhibition (Fig. 6F), as previously reported (50,51).

Blocking TGFβ increases DC maturation and antigen-presentation capacity

To further examine monocyte lineage differentiation upon TGFβ blockade, we used CyTOF analysis of populations using unsupervised clustering and visualization as a force-directed graph (30). A separate group of clusters were evident in the presence of TGFβ inhibitor (Fig. 7A), which was characterized by lower CD11b and high expression of CD14, CD11c, HLA-DR and CD38, which are indicative of antigen-presenting DC (52) (Fig. 7B, Supplementary Fig. S9A). We confirmed that DC maturation and activation markers HLA-1, HLA-DR, CD86, and CD11c were significantly increased after treatment with LY2109761 (Fig. 7C). Mature HLA^+ DCs were increased when TGFβ ligand was blocked using neutralizing antibody 1D11 (Fig. 7D). TGFβ inhibition increased the gene expression of the molecules involved with antigen-presentation: *HLA-A*, *HLA-DRA*, *HLA-DRB*, and *B2M*, indicative of greater antigen-presenting capacity (Supplementary Fig. S9B). The expression of HLA-DR was validated by flow cytometry. TGFβ inhibition significantly increased cell surface HLA-DR and HLA-1 compared to cytokine alone-treated cells (Supplementary Fig. S9C,D).

To functionally test the antigen-presentation capacity of the resulting cells, we co-cultured $CD11b^+$ cells with autologous naïve $CD3^+$ T-cells and a human lung cancer cell line (NCI-H1299). We assessed activity of cytotoxic T cells by measuring tumor cell apoptosis (Supplementary Fig. S10A). $CD11b^+$ cells cultured in the presence of the cytokines GM-CSF and IL6 were less efficient at priming naïve T cells compared to those treated with LY2109761. The enhanced priming of T cells resulted in increased tumor cell killing, measured by either the percentage or the intensity of annexin V^+ tumor cells (Fig. 7E–H). The cross-talk between myeloid cells and T cells mediated the increase because naïve T cells or myeloid cells alone were inefficient at eliciting tumor cell apoptosis (Supplementary Fig. S10B, C). These results collectively indicate that monocyte autocrine TGFβ supported generation of immunosuppressive MDSCs, whereas inhibition of TGFβ signaling or ligand blockade promoted lineage commitment to macrophages and antigen-presenting DCs, which promote antitumor immunity.

Discussion

Using $CD14^+$ monocytes from normal blood, we asked how TGFβ, a prominent cytokine in cancer, affects lineage commitment. Gene expression profiles revealed that TGFβ is a survival factor, without which monocytes undergo rapid apoptotic death. Both autocrine and paracrine TGFβ regulated myeloid lineage commitment by promoting monocyte survival and endorsing differentiation to MDSCs at the expense of antigen-presenting DCs and macrophages. Although MDSCs identified by cell surface markers are neither homogeneous nor acting alone, this population is an important part of a network of innate immune cells in cancer that impede adaptive immunity by shifting T-cell lineages and skewing the TME towards immunosuppression.

Our studies revealed that autocrine TGFβ enforces human MDSC differentiation as well as their immunosuppressive potential, consistent with prior studies implicating TGFβ in MDSC

generation in murine inflammatory models (53). Our experiments using isolated $CD14^+$ cells expand on previous reports using PBMCs to study conditions favoring MDSC generation (14,54). We determined that exogenous TGFβ increased autocrine TGFβ activation that is crucial for MDSC function. Consistent with this, TGFβ-induced MDSCs had greater capacity to suppress cytotoxic $CD8^+$ T-cells. TGFβ production by MDSCs suppresses T-cell responses (8,9). This shift, accompanied by a significant increase in inflammatory cytokines and expression of antigen-presenting molecules, could increase the efficiency of an antitumor immune response (55). This interplay was evident in that TGFβ-generated MDSCs both inhibited T-cell proliferation and increased the frequency of Treg, which are an additional source of TGFβ (56).

The high activity of TGFβ in the TME likely promotes monocyte recruitment (7), and regulates macrophage polarization, skewing differentiation towards an M2 tumor-promoting phenotype (51,57). TGFβ is also implicated in the reprograming of PMN-MDSCs or tumor-associated neutrophils with immunosuppressive capacity (58). Interestingly, TGFβ regulates micro-RNA miR-494, which promotes MDSC accumulation in murine cancer models (59). As both chemotherapy and radiation therapy rapidly and persistently stimulate TGFβ activity in cancers (3,4,60,61), treatment could further increase monocyte survival and promote an immunosuppressive TME in a manner that compromises the response to immunotherapy. Studies of patients who do not respond to checkpoint blockade suggest that TGFβ represents a major obstacle (4–6).

Targeting the increase in MDSCs observed in cancer patients has been proposed as a strategy to prevent tumor progression (62). One model for MDSC accumulation in cancer patients suggests two signals are needed: the first expands myeloid progenitors and arrests terminal differentiation, followed by a second signal that endorses immunosuppressive activity and converts the immature myeloid cells into functional MDSCs (8,9). Here, we showed that TGFβ executed both steps: the amplification of myeloid precursors via increased survival and differentiation into immunosuppressive MDSCs. Autocrine TGFβ is essential to maintenance of this differentiation block, thus, raising the potential of TGFβ inhibitors to release the immunosuppressive TME via multiple mechanisms.

The translational potential of these findings is supported by demonstration that inhibiting TGFβ could re-orient monocyte differentiation towards pro-inflammatory and antigen-presenting macrophages and DCs. Viable TGFβ inhibition therapies are in clinical trials for treatment of various diseases including cancer (63,64). The abundance of MDSCs in cancer correlates with resistance to checkpoint inhibitors (65–68), as well as with poor responses to standard of care treatment (69). Our studies showing that high active TGFβ could skew monocyte differentiation supports the proposition that clinical strategies employing TGFβ inhibitors in cancer could reprogram the myeloid component to potentiate responses to immunotherapy.

Supplementary Material

Refer to Web version on PubMed Central for supplementary material.

Acknowledgements

This work was supported by Eli Lilly and Company through the Lilly Research Award Program, Varian Medical Systems, Inc., and NIH DP5OD023056 to MHS. RR was supported by National Cancer Institute Cancer Center Support Grant (5P30CA082103).

Authors would like to thank Dr. David Schaer for helpful suggestions, and Mr. William Chou and Ms. Xiaohong Xu for technical support. We also thank Dr. Ann Lazar for advice on biostatistics and data analysis. We thank members of the NYUMC Genome technology center, which is partially supported by the Cancer Center Support Grant, P30CA016087, at the Laura and Isaac Perlmutter Cancer Center. The CyTOF mass cytometer at UCSF was supported by NIH grant S10OD018040.

Funding: This work was supported by Eli Lilly and Company through the Lilly Research Award Program (MHBH, AGJ), Varian Medical Systems, Inc. (MHBH, SD, CHL, IP), NIH DP5OD023056 (MHS, IT, DMM), National Cancer Institute Cancer Center Support Grant 5P30CA082103 (RR). The CyTOF mass cytometer at UCSF was supported by NIH grant S10OD018040.

Disclosure of Conflicts of Interest

AGJ, IP, SD, CHL, RR, IT, DMH and MHS have no conflicts to disclose. MHBH received from funding from, and KED is an employee of, Eli Lilly and Co. RP is employee from Varian Medical Systems.

References

1. Pickup M, Novitskiy S, Moses HL. The roles of TGFbeta in the tumour microenvironment. Nat Rev Cancer 2013;13(11):788–99 doi 10.1038/nrc3603. [PubMed: 24132110]
2. Massagué J TGF[beta] in Cancer. Cell 2008;134(2):215–30. [PubMed: 18662538]
3. Du S, Bouquet F, Lo C- H, Pellicciotta I, Bolourchi S, Parry R, et al. Attenuation of the DNA Damage Response by TGFβ Inhibitors Enhances Radiation Sensitivity of NSCLC Cells In Vitro and In Vivo Int J Radiat Oncol Biol Phys 2014;91(1):91–9 doi 10.1016/j.ijrobp.2014.09.026.
4. Vanpouille-Box C, Diamond J, Pilones KA, Zavadil J, Babb JS, Formenti SC, et al. Transforming growth factor (TGF) β is a master regulator of radiotherapy-induced anti-tumor immunity. Cancer research 2015;75(11):2232–42 doi 10.1158/0008-5472.CAN-14-3511. [PubMed: 25858148]
5. Mariathasan S, Turley SJ, Nickles D, Castiglioni A, Yuen K, Wang Y, et al. TGFbeta attenuates tumour response to PD-L1 blockade by contributing to exclusion of T cells. Nature 2018;554(7693): 544–8 doi 10.1038/nature25501. [PubMed: 29443960]
6. Tauriello DVF, Palomo-Ponce S, Stork D, Berenguer-Llergo A, Badia-Ramentol J, Iglesias M, et al. TGFbeta drives immune evasion in genetically reconstituted colon cancer metastasis. Nature 2018;554(7693):538–43 doi 10.1038/nature25492. [PubMed: 29443964]
7. Wahl SM, Hunt DA, Wakefield LM, McCartney-Francis N, Wahl M, Roberts AB, et al. Transforming growth-factor beta (TGF-beta) induces monocyte chemotaxis an growth factor production. Proc Natl Acad Sci USA 1987;84:5788–91. [PubMed: 2886992]
8. Gabrilovich DI. Myeloid-Derived Suppressor Cells. Cancer immunology research 2017;5(1):3–8 doi 10.1158/2326-6066.cir-16-0297. [PubMed: 28052991]
9. Condamine T, Gabrilovich DI. Molecular mechanisms regulating myeloid-derived suppressor cell differentiation and function. Trends Immunol 2011;32(1):19–25 doi 10.1016/j.it.2010.10.002. [PubMed: 21067974]
10. Bronte V, Brandau S, Chen SH, Colombo MP, Frey AB, Greten TF, et al. Recommendations for myeloid-derived suppressor cell nomenclature and characterization standards. Nature communications 2016;7:12150 doi 10.1038/ncomms12150.
11. Marvel D, Gabrilovich DI. Myeloid-derived suppressor cells in the tumor microenvironment: expect the unexpected. J Clin Invest 2015;125(9):3356–64 doi 10.1172/JCI80005. [PubMed: 26168215]
12. Gabrilovich DI, Nagaraj S. Myeloid-derived suppressor cells as regulators of the immune system. Nat Rev Immunol 2009;9(3):162–74 doi nri2506 [pii] 10.1038/nri2506. [PubMed: 19197294]

13. Zhang S, Ma X, Zhu C, Liu L, Wang G, Yuan X. The Role of Myeloid-Derived Suppressor Cells in Patients with Solid Tumors: A Meta-Analysis. PloS one 2016;11(10):e0164514 doi 10.1371/journal.pone.0164514. [PubMed: 27780254]
14. Lechner MG, Liebertz DJ, Epstein AL. Characterization of cytokine-induced myeloid-derived suppressor cells from normal human peripheral blood mononuclear cells. Journal of immunology 2010;185(4):2273–84 doi 10.4049/jimmunol.1000901.
15. Cerami E, Gao J, Dogrusoz U, Gross BE, Sumer SO, Aksoy BA, et al. The cBio cancer genomics portal: an open platform for exploring multidimensional cancer genomics data. Cancer discovery 2012;2(5):401–4 doi 10.1158/2159-8290.CD-12-0095. [PubMed: 22588877]
16. Gao J, Aksoy BA, Dogrusoz U, Dresdner G, Gross B, Sumer SO, et al. Integrative analysis of complex cancer genomics and clinical profiles using the cBioPortal. Science signaling 2013;6(269):pl1 doi 10.1126/scisignal.2004088. [PubMed: 23550210]
17. Bengtsson H, Simpson K, Bullard J, Hansen K. aroma.affymetrix: A generic framework in R for analyzing small to very large Affymetrix data sets in bounded memory. University of California, Berkeley 2008 2 2008.
18. Huber W, Carey VJ, Gentleman R, Anders S, Carlson M, Carvalho BS, et al. Orchestrating high-throughput genomic analysis with Bioconductor. Nature methods 2015;12(2):115–21 doi 10.1038/nmeth.3252. [PubMed: 25633503]
19. R Core Team. R: A language and environment for statistical computing. Vienna, Austria R Foundation for Statistical Computing; 2015.
20. Robinson MD, McCarthy DJ, Smyth GK. edgeR: a Bioconductor package for differential expression analysis of digital gene expression data. Bioinformatics 2010;26(1):139–40 doi 10.1093/bioinformatics/btp616. [PubMed: 19910308]
21. Law CW, Chen Y, Shi W, Smyth GK. voom: Precision weights unlock linear model analysis tools for RNA-seq read counts. Genome biology 2014;15(2):R29 doi 10.1186/gb-2014-15-2-r29. [PubMed: 24485249]
22. Smyth GK. Linear models and empirical bayes methods for assessing differential expression in microarray experiments. Statistical applications in genetics and molecular biology 2004;3:Article3 doi 10.2202/1544-6115.1027.
23. Ritchie ME, Phipson B, Wu D, Hu Y, Law CW, Shi W, et al. limma powers differential expression analyses for RNA-sequencing and microarray studies. Nucleic acids research 2015;43(7):e47 doi 10.1093/nar/gkv007. [PubMed: 25605792]
24. Storey D, Bass A, Dabney A, Robinson D. qvalue: Q-value estimation for false discovery rate control. R package version 2.4.22015.
25. Wu D, Lim E, Vaillant F, Asselin-Labat ML, Visvader JE, Smyth GK. ROAST: rotation gene set tests for complex microarray experiments. Bioinformatics 2010;26(17):2176–82 doi 10.1093/bioinformatics/btq401. [PubMed: 20610611]
26. Subramanian A, Tamayo P, Mootha VK, Mukherjee S, Ebert BL, Gillette MA, et al. Gene set enrichment analysis: a knowledge-based approach for interpreting genome-wide expression profiles. Proceedings of the National Academy of Sciences of the United States of America 2005;102(43):15545–50 doi 10.1073/pnas.0506580102. [PubMed: 16199517]
27. Pellicciotta I, Marciscano AE, Hardee ME, Francis D, Formenti S, Barcellos-Hoff MH. Development of a novel multiplexed assay for quantification of transforming growth factor-β (TGFβ). Growth Factors 2014;33(2):79–91 doi 10.3109/08977194.2014.999367.
28. Fienberg HG, Simonds EF, Fantl WJ, Nolan GP, Bodenmiller B. A platinum-based covalent viability reagent for single-cell mass cytometry. Cytometry Part A : the journal of the International Society for Analytical Cytology 2012;81(6):467–75 doi 10.1002/cyto.a.22067. [PubMed: 22577098]
29. Spitzer MH, Nolan GP. Mass Cytometry: Single Cells, Many Features. Cell 2016;165(4):780–91 doi 10.1016/j.cell.2016.04.019. [PubMed: 27153492]
30. Spitzer MH, Gherardini PF, Fragiadakis GK, Bhattacharya N, Yuan RT, Hotson AN, et al. IMMUNOLOGY. An interactive reference framework for modeling a dynamic immune system. Science (New York, NY) 2015;349(6244):1259425 doi 10.1126/science.1259425.

31. Gentles AJ, Newman AM, Liu CL, Bratman SV, Feng W, Kim D, et al. The prognostic landscape of genes and infiltrating immune cells across human cancers. Nature medicine 2015;21(8):938–45 doi 10.1038/nm.3909.
32. Newman AM, Liu CL, Green MR, Gentles AJ, Feng W, Xu Y, et al. Robust enumeration of cell subsets from tissue expression profiles. Nature methods 2015;12(5):453–7 doi 10.1038/nmeth.3337. [PubMed: 25822800]
33. Koinuma D, Tsutsumi S, Kamimura N, Taniguchi H, Miyazawa K, Sunamura M, et al. Chromatin immunoprecipitation on microarray analysis of Smad2/3 binding sites reveals roles of ETS1 and TFAP2A in transforming growth factor beta signaling. Molecular and cellular biology 2009;29(1):172–86 doi 10.1128/mcb.01038-08. [PubMed: 18955504]
34. Plasari G, Calabrese A, Dusserre Y, Gronostajski RM, McNair A, Michalik L, et al. Nuclear factor I-C links platelet-derived growth factor and transforming growth factor beta1 signaling to skin wound healing progression. Molecular and cellular biology 2009;29(22):6006–17 doi 10.1128/mcb.01921-08. [PubMed: 19752192]
35. Fulcher JA, Hashimi ST, Levroney EL, Pang M, Gurney KB, Baum LG, et al. Galectin-1-matured human monocyte-derived dendritic cells have enhanced migration through extracellular matrix. Journal of immunology 2006;177(1):216–26.
36. Foster SL, Hargreaves DC, Medzhitov R. Gene-specific control of inflammation by TLR-induced chromatin modifications. Nature 2007;447(7147):972–8 doi 10.1038/nature05836. [PubMed: 17538624]
37. Himes SR, Cronau S, Mulford C, Hume DA. The Runx1 transcription factor controls CSF-1-dependent and -independent growth and survival of macrophages. Oncogene 2005;24(34):5278–86 doi 10.1038/sj.onc.1208657. [PubMed: 16007221]
38. Tiwari N, Tiwari VK, Waldmeier L, Balwierz PJ, Arnold P, Pachkov M, et al. Sox4 is a master regulator of epithelial-mesenchymal transition by controlling Ezh2 expression and epigenetic reprogramming. Cancer Cell 2013;23(6):768–83 doi 10.1016/j.ccr.2013.04.020. [PubMed: 23764001]
39. Liebermann DA, Hoffman B. Gadd45 in the response of hematopoietic cells to genotoxic stress. Blood cells, molecules & diseases 2007;39(3):329–35 doi 10.1016/j.bcmd.2007.06.006.
40. Guo H, Callaway JB, Ting JP. Inflammasomes: mechanism of action, role in disease, and therapeutics. Nature medicine 2015;21(7):677–87 doi 10.1038/nm.3893.
41. Goyal A, Wang Y, Graham MM, Doseff AI, Bhatt NY, Marsh CB. Monocyte survival factors induce Akt activation and suppress caspase-3. American journal of respiratory cell and molecular biology 2002;26(2):224–30 doi 10.1165/ajrcmb.26.2.4640. [PubMed: 11804874]
42. Song G, Ouyang G, Bao S. The activation of Akt/PKB signaling pathway and cell survival. Journal of cellular and molecular medicine 2005;9(1):59–71. [PubMed: 15784165]
43. Wang T, Niu G, Kortylewski M, Burdelya L, Shain K, Zhang S, et al. Regulation of the innate and adaptive immune responses by Stat-3 signaling in tumor cells. Nature medicine 2004;10:48–54.
44. Sinha P, Okoro C, Foell D, Freeze HH, Ostrand-Rosenberg S, Srikrishna G. Proinflammatory S100 proteins regulate the accumulation of myeloid-derived suppressor cells. Journal of immunology 2008;181(7):4666–75.
45. Cheng P, Corzo CA, Luetteke N, Yu B, Nagaraj S, Bui MM, et al. Inhibition of dendritic cell differentiation and accumulation of myeloid-derived suppressor cells in cancer is regulated by S100A9 protein. The Journal of experimental medicine 2008;205(10):2235–49 doi 10.1084/jem.20080132. [PubMed: 18809714]
46. Rodon L, Gonzalez-Junca A, Inda Mdel M, Sala-Hojman A, Martinez-Saez E, Seoane J. Active CREB1 promotes a malignant TGFbeta2 autocrine loop in glioblastoma. Cancer discovery 2014;4(10):1230–41 doi 10.1158/2159-8290.CD-14-0275. [PubMed: 25084773]
47. Gonzalez-Navajas JM, Lee J, David M, Raz E. Immunomodulatory functions of type I interferons. Nat Rev Immunol 2012;12(2):125–35 doi 10.1038/nri3133. [PubMed: 22222875]
48. Sim GC, Radvanyi L. The IL-2 cytokine family in cancer immunotherapy. Cytokine & growth factor reviews 2014;25(4):377–90 doi 10.1016/j.cytogfr.2014.07.018. [PubMed: 25200249]
49. Liu M, Guo S, Stiles JK. The emerging role of CXCL10 in cancer (Review). Oncol Lett 2011;2(4):583–9 doi 10.3892/ol.2011.300. [PubMed: 22848232]

50. Gong D, Shi W, Yi SJ, Chen H, Groffen J, Heisterkamp N. TGFbeta signaling plays a critical role in promoting alternative macrophage activation. BMC Immunol 2012;13:31 doi 10.1186/1471-2172-13-31. [PubMed: 22703233]
51. Mantovani A, Sozzani S, Locati M, Allavena P, Sica A. Macrophage polarization: tumor-associated macrophages as a paradigm for polarized M2 mononuclear phagocytes. Trends in Immunology 2002;23(11):549–55. [PubMed: 12401408]
52. Fedele G, Frasca L, Palazzo R, Ferrero E, Malavasi F, Ausiello CM. CD38 is expressed on human mature monocyte-derived dendritic cells and is functionally involved in CD83 expression and IL-12 induction. European journal of immunology 2004;34(5):1342–50 doi 10.1002/eji.200324728. [PubMed: 15114667]
53. Lee CR, Kwak Y, Yang T, Han JH, Park SH, Ye MB, et al. Myeloid-Derived Suppressor Cells Are Controlled by Regulatory T Cells via TGF-beta during Murine Colitis. Cell reports 2016;17(12):3219–32 doi 10.1016/j.celrep.2016.11.062. [PubMed: 28009291]
54. Lechner MG, Megiel C, Russell SM, Bingham B, Arger N, Woo T, et al. Functional characterization of human Cd33+ and Cd11b+ myeloid-derived suppressor cell subsets induced from peripheral blood mononuclear cells co-cultured with a diverse set of human tumor cell lines. Journal of translational medicine 2011;9:90 doi 10.1186/1479-5876-9-90. [PubMed: 21658270]
55. Kao JY, Gong Y, Chen CM, Zheng QD, Chen JJ. Tumor-derived TGF-beta reduces the efficacy of dendritic cell/tumor fusion vaccine. Journal of immunology 2003;170(7):3806–11.
56. Liu VC, Wong LY, Jang T, Shah AH, Park I, Yang X, et al. Tumor evasion of the immune system by converting CD4+CD25− T cells into CD4+CD25+ T regulatory cells: role of tumor-derived TGF-b. Journal of immunology 2007;178(5):2883–92.
57. Yang WC, Ma G, Chen SH, Pan PY. Polarization and reprogramming of myeloid-derived suppressor cells. Journal of molecular cell biology 2013;5(3):207–9 doi 10.1093/jmcb/mjt009. [PubMed: 23532593]
58. Fridlender ZG, Sun J, Kim S, Kapoor V, Cheng G, Ling L, et al. Polarization of Tumor-Associated Neutrophil Phenotype by TGF-b N1 versus N2 TAN. Cancer Cell 2009;16(3):183–94. [PubMed: 19732719]
59. Liu Y, Lai LH, Chen QY, Song YJ, Xu S, Ma F, et al. MicroRNA-494 Is Required for the Accumulation and Functions of Tumor-Expanded Myeloid-Derived Suppressor Cells via Targeting of PTEN. Journal of immunology 2012;188(11):5500–10 doi 10.4049/jimmunol.1103505.
60. Hardee ME, Marciscano AE, Medina-Ramirez CM, Zagzag D, Narayana A, Lonning SM, et al. Resistance of Glioblastoma-Initiating Cells to Radiation Mediated by the Tumor Microenvironment Can Be Abolished by Inhibiting Transforming Growth Factor-β. Cancer research 2012;72(16):4119–29. [PubMed: 22693253]
61. Bouquet SF, Pal A, Pilones KA, Demaria S, Hann B, Akhurst RJ, et al. Transforming growth factor b1 inhibition increases the radiosensitivity of breast cancer cells in vitro and promotes tumor control by radiation in vivo. Clin Cancer Res 2011;17(21):6754–65 doi 10.1158/1078-0432.CCR-11-0544. [PubMed: 22028490]
62. Ugel S, Delpozzo F, Desantis G, Papalini F, Simonato F, Sonda N, et al. Therapeutic targeting of myeloid-derived suppressor cells. Current opinion in pharmacology 2009;9(4):470–81 doi 10.1016/j.coph.2009.06.014. [PubMed: 19616475]
63. Akhurst RJ, Hata A. Targeting the TGFb signalling pathway in disease. Nat Rev Drug Discov 2012;11(10):790–811. [PubMed: 23000686]
64. Rodon J, Carducci MA, Sepulveda-Sanchez JM, Azaro A, Calvo E, Seoane J, et al. First-in-Human Dose Study of the Novel Transforming Growth Factor-beta Receptor I Kinase Inhibitor LY2157299 Monohydrate in Patients with Advanced Cancer and Glioma. Clin Cancer Res 2015;21(3):553–60 doi 10.1158/1078-0432.ccr-14-1380. [PubMed: 25424852]
65. Dammeijer F, Lau SP, van Eijck CHJ, van der Burg SH, Aerts J. Rationally combining immunotherapies to improve efficacy of immune checkpoint blockade in solid tumors. Cytokine & growth factor reviews 2017;36:5–15 doi 10.1016/j.cytogfr.2017.06.011. [PubMed: 28693973]
66. De Henau O, Rausch M, Winkler D, Campesato LF, Liu C, Cymerman DH, et al. Overcoming resistance to checkpoint blockade therapy by targeting PI3Kgamma in myeloid cells. Nature 2016;539(7629):443–7 doi 10.1038/nature20554. [PubMed: 27828943]

67. Lu X, Horner JW, Paul E, Shang X, Troncoso P, Deng P, et al. Effective combinatorial immunotherapy for castration-resistant prostate cancer. Nature 2017;543(7647):728–32 doi 10.1038/nature21676. [PubMed: 28321130]

68. Sade-Feldman M, Kanterman J, Klieger Y, Ish-Shalom E, Olga M, Saragovi A, et al. Clinical Significance of Circulating CD33+CD11b+HLA-DR-Myeloid Cells in Patients with Stage IV Melanoma Treated with Ipilimumab. Clin Cancer Res 2016;22(23):5661–72 doi 10.1158/1078-0432.CCR-15-3104. [PubMed: 27178742]

69. Tada K, Kitano S, Shoji H, Nishimura T, Shimada Y, Nagashima K, et al. Pretreatment Immune Status Correlates with Progression-Free Survival in Chemotherapy-Treated Metastatic Colorectal Cancer Patients. Cancer immunology research 2016;4(7):592–9 doi 10.1158/2326-6066.CIR-15-0298. [PubMed: 27197061]

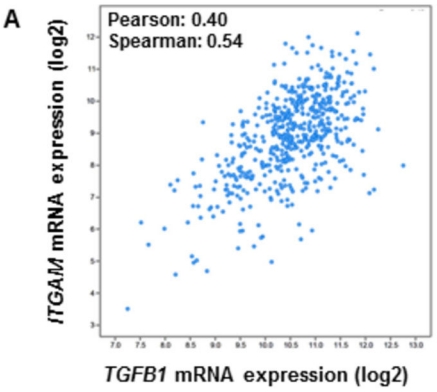

B

Marker	Cell type	Pearson	Spearman	P value
ITGAM(CD11b)	Monocyte	0.40	0.54	<0.0001
CD14	Monocyte	0.36	0.45	<0.0001
CD33	Monocyte	0.38	0.51	<0.0001
CSF1R	Monocytes	0.47	0.58	<0.0001
CEACAM8(CD66b)	Granulocytes	0.04	0.16	0.3057
ITGAX(CD11c)	Dendritic cells	0.32	0.43	<0.0001
ITGAE(CD103)	DC	0.031	0.095	0.4770
NCAM1(CD56)	NK	-0.1	0.132	0.0222

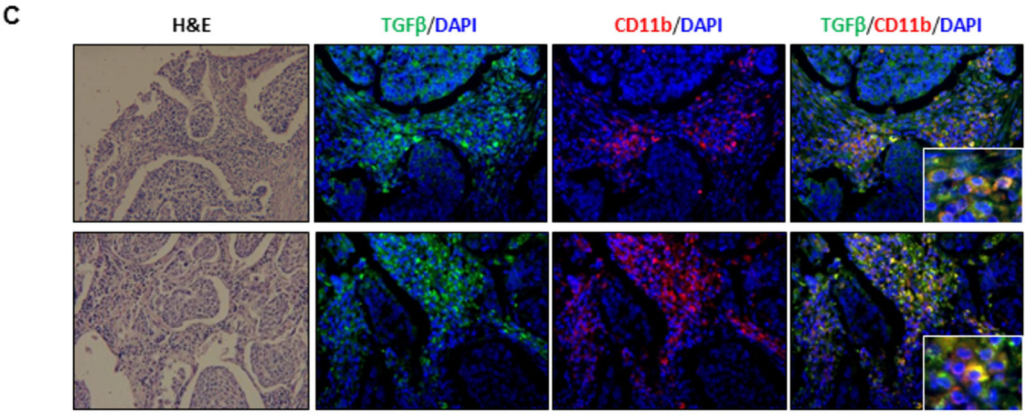

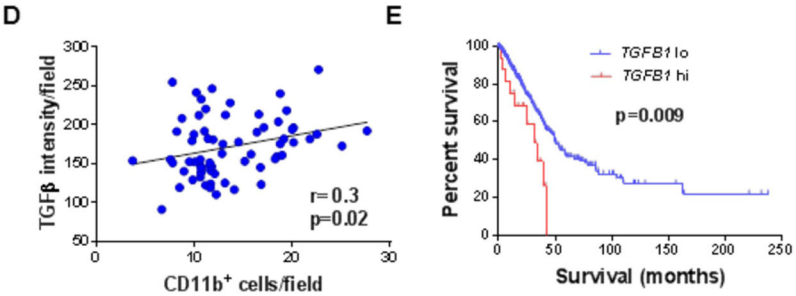

Fig. 1. TGFβ expression correlates with myeloid cell markers in TCGA human cancers.

A. cBioportal for cancer genomics (15,16) was used to assess the correlation between *TGFB1* gene expression and myeloid cell marker CD11b (*ITGAM*) in TCGA NSCLC (N=586) and Pearson and Spearman correlations were calculated. **B.** cBioportal was used to test correlations between expression of *TGFB1* and myeloid cell markers *CD14*, *CD33, CSF1R,* CD11c (*ITGAX*) and *CD103*, NK cell marker CD56 (*NCAM1*), and neutrophil/ granulocyte marker CD66b (*CEACAM8*) using TCGA NSCLC adenocarcinoma specimens (N=586) (ns= not statistically significant correlation). **C.** Examples of NSCLC tissue microarray stained for active TGFβ (green) and CD11b (red). DAPI (blue) was used to stain the nuclei. **D.** Correlation between CD11b and TGFβ activity immunostaining in NSCLC tissue array (N=66 samples, p=0.02; Pearson, Spearman=0.3). **E.** Kaplan Meyer survival curves of TCGA NSCLC patients stratified according to the expression of *TGFB1* (z-score

threshold=2; N=514 patients *TGFB1*hi, N=514 patients *TGFB1*lo). HR=3.4. Median survival=49.8 mo (*TGFB1*lo) vs 32.4 mo (*TGFB1*hi).

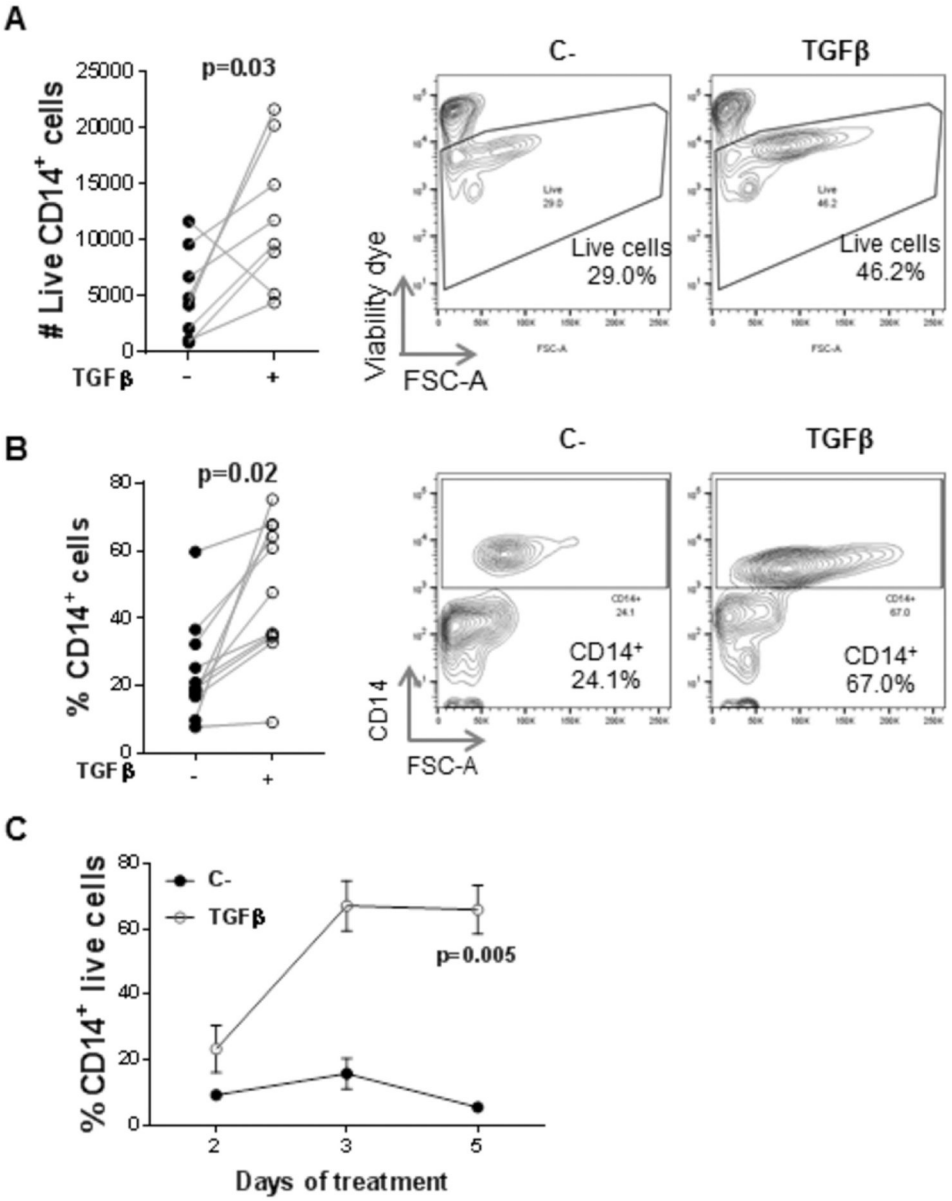

Fig. 2. TGFβ treatment increases CD14$^+$ monocytes.

A. Number of CD14$^+$ live cells in control (C., solid circles) or TGFβ-treated samples (TGFβ, open circles) (N=8 donors in 4 independent experiments). Representative FACS profile is shown in the right panels. **B.** Percentage of CD14$^+$ cells in cultures treated with TGFβ for 5 days (open circles) (N=11). Representative FACS profiles are shown on the right. **C.** Percentage of CD14$^+$ live cells measured at indicated time points treated with TGFβ (open circles) or without (solid circles) (N=3 donors). p=0.005 (2 way-ANOVA).

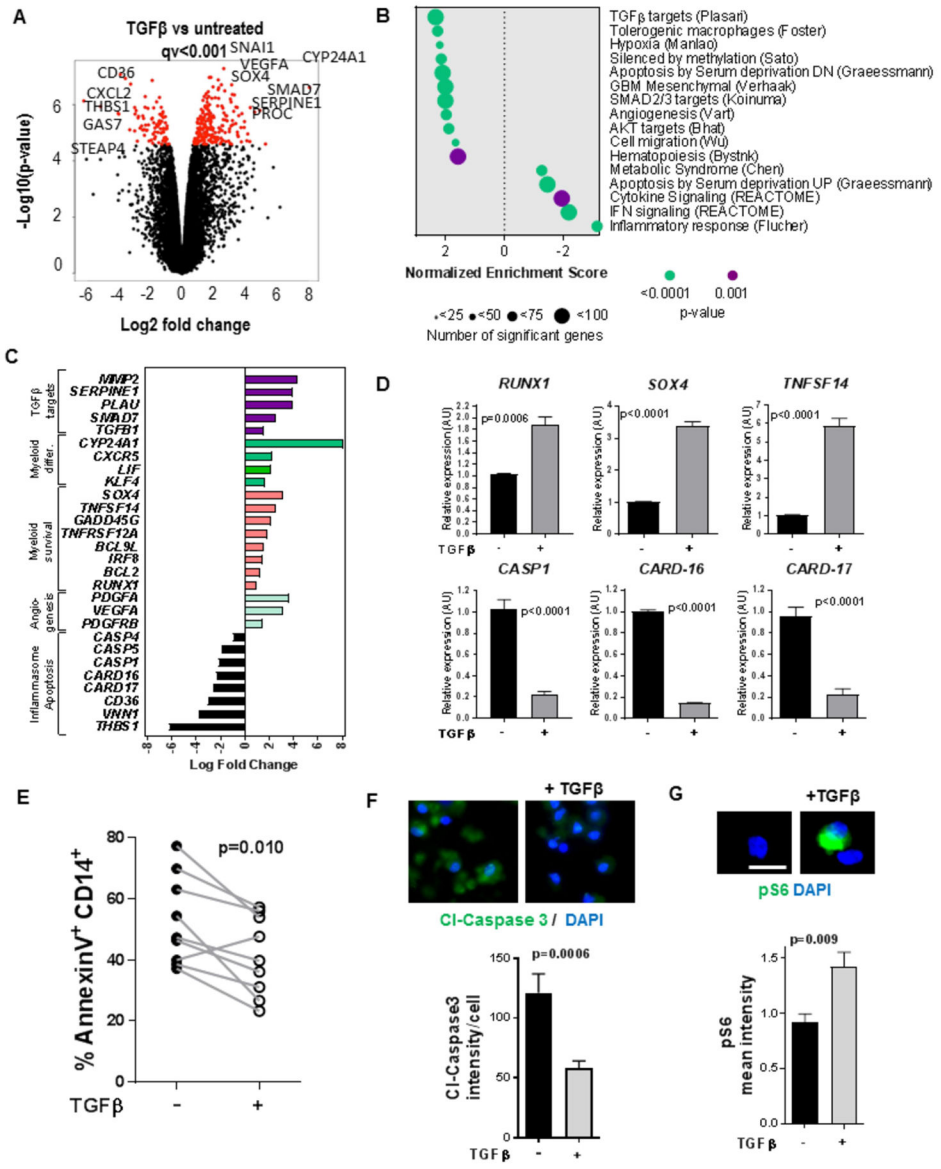

Fig. 3. TGFβ regulates survival and differentiation pathways in CD14$^+$ cells.

A. Volcano plot showing the top differentially regulated genes in TGFβ-treated or untreated CD14$^+$ cells after 8 hours of culture. Red dots correspond to the differentially expressed genes with q-value < 0.001 (3412/18047 total; 3127/14956 unique). **B.** Summary of the main pathways significantly correlated with TGFβ treatment ranked by NES obtained by GSEA. **C.** List of selected target genes significantly upregulated or downregulated after TGFβ treatment. Genes are grouped according to their biological function. **D.** Validation of some of TGFβ-regulated genes using qRT-PCR (N=3). Gene expression was normalized using *GAPDH* and *RPL13* and expressed as relative to untreated cells in arbitrary units (AU). Mean and SEM are shown. **E.** Percentage of CD14$^+$ cells incorporating annexinV after 24 hours (N=9). **F.** Representative images of cleaved caspase-3 immunofluorescence on CD14$^+$ monocytes without (left) or with TGFβ for 24 hours. Fluorescence intensity per cell was quantified using ImageJ (N=4). **G.** Representative images of CD14$^+$ cell pS6 ribosomal

protein immunofluorescence are shown. Fluorescence intensity was quantified using ImageJ (N=3).

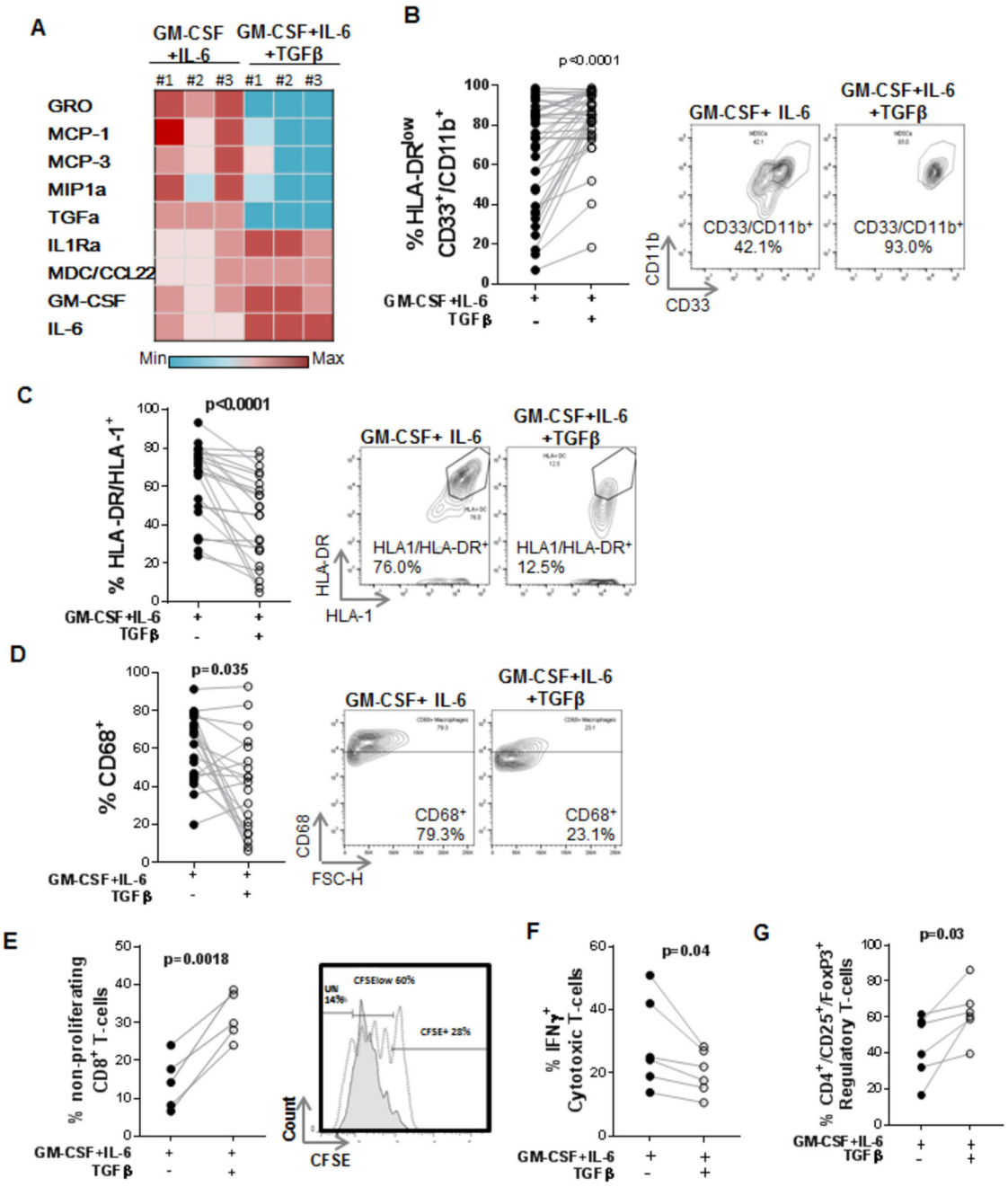

Fig. 4. TGFβ increases cells with MDSC markers, MDSC-related genes, and immunosuppressive function.

A. CD14$^+$ selected cells were treated for 48 hours with the combination of GM-CSF and IL6 with or without TGFβ (N=3). A multiplexed panel of cytokines and chemokines was used to assay the conditioned media after 48 hours. Heatmap representing the relative protein concentration of selected cytokines and chemokines. Normalized protein concentrations are shown in Supplementary Fig. S2. **B.** Percentage of live HLA-DR^{low}CD11b$^+$CD33$^+$ cells after being cultured for 5 days with GMCSF+IL6 and adding TGFβ (open circles). MDSCs were quantified within the live CD45$^+$ leukocyte and CD14$^+$ population (N=36).

Representative FACS plots of $CD11b^+CD33^+$ within the $CD14^+HLA\text{-}DR^{low}$ population are shown in the right panels. **C.** Percentage of $HLA\text{-}DR^+HLA\text{-}1^+$ mature antigen-presenting cells (mDCs) after being cultured for 5 days with GM-CSF+IL6 and with the addition of TGFβ (open circles) (N=23). Representative FACS plots showing double positive HLA-DR and HLA-1 mature DCs within the $CD45^+$ population are shown in the right panels. **D.** Percentage of $CD68^+$ macrophages after being cultured for 5 days with GM-CSF+IL6 and adding TGFβ (open circles) (N=20). **E.** Immunosuppressive assay was performed, as depicted in Supplementary Fig. S5C. T-cell proliferation was assessed by CFSE staining after $CD3^+$ T-cells were co-cultured with equal number of $CD11b^+$ MDSC that had been generated under the conditions indicated. Percentage of $CFSE^+$ non-proliferating $CD8^+$ T-cells was used as readout for the immunosuppressive potential of MDSC as a function of TGFβ (open circles) (N=5). Grey shadowed area shows CFSE intensity of T-cells co-cultured with GM-CSF/IL6-induced MDSCs. Dotted line shows the CFSE intensity of T-cells after co-culture with MDSCs generated in the presence of cytokines plus TGFβ. **F.** Percentage of $IFN\gamma^+$ active $CD8^+$ cytotoxic T-cells was measured after co-culture with myeloid cells that had been generated under the listed conditions (N=6). **G.** Percentage of $CD4^+FoxP3^+$ Tregs was measured after co-culture with myeloid cells that had been generated under the listed conditions (N=6).

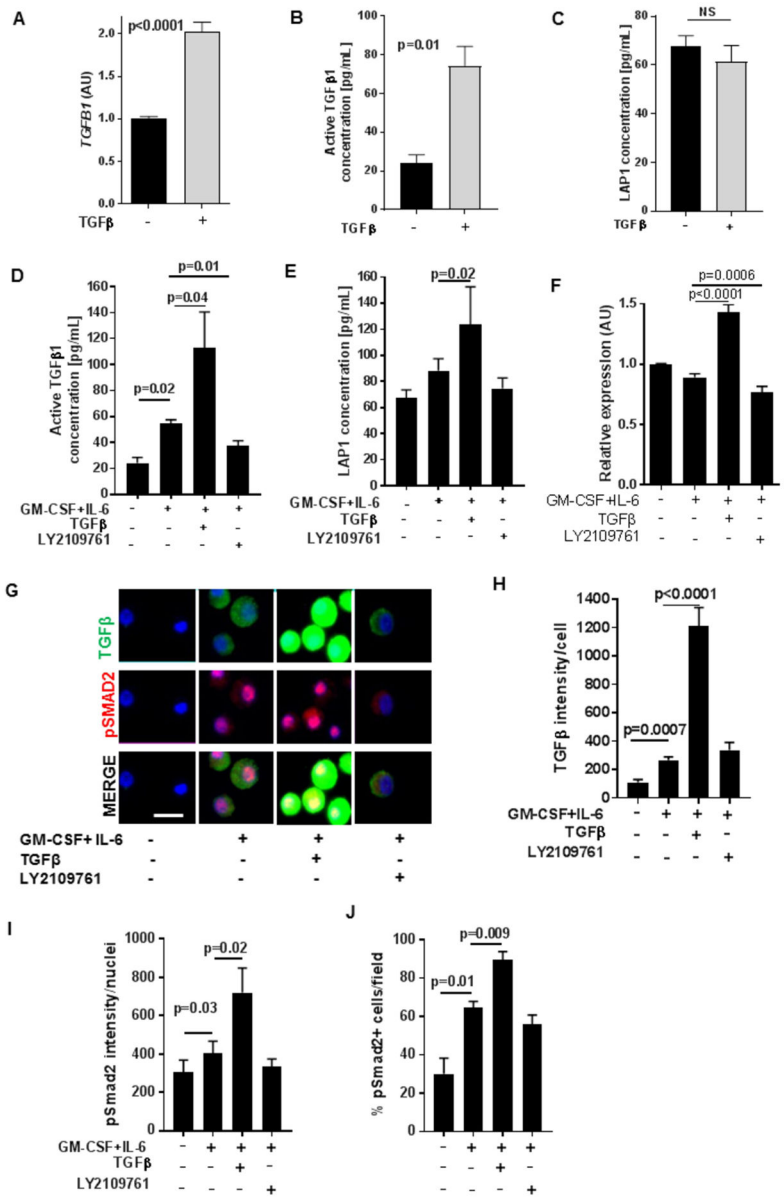

Fig. 5. TGFβ-treated myeloid cells activate more TGFβ

A. *TGFB1* mRNA expression of $CD14^+$ cells after 4 hours of TGFβ treatment measured by qRT-PCR relative to untreated cells (N=3). **B.** Active TGFβ1 protein concentration measured in supernatants of $CD14^+$ cells treated with TGFβ for 48 hours (N=3). **C.** Latent TGFβ1 was measured by MSD in supernatants of $CD14^+$ cells treated with or without TGFβ for 48 hours (N=3). **D.** Active TGFβ1 was measured by MSD assay in supernatants of $CD14^+$ cells treated with cytokines (GM-CSF+IL6) and either TGFβ or a TβRI inhibitor, LY2109761 (N=3). **E.** Latent TGFβ1 was measured by MSD in supernatants of $CD14^+$ cells treated as in D (N=3). **F.** *TGFB1* mRNA expression on $CD14^+$ cells treated as in D,E. **G.** $CD14^+$ cells were stained with antibodies that selectively detect active TGFβ1 (green) and pSMAD2 (red). DAPI was used to counterstain the nuclei. **H.** Mean fluorescence intensity of TGFβ

was measured (N=3). **I.** Nuclear fluorescence intensity of phosphorylated-SMAD2 was measured (N=3). **J.** The frequency of pSMAD positive nuclei was determined (N=3).

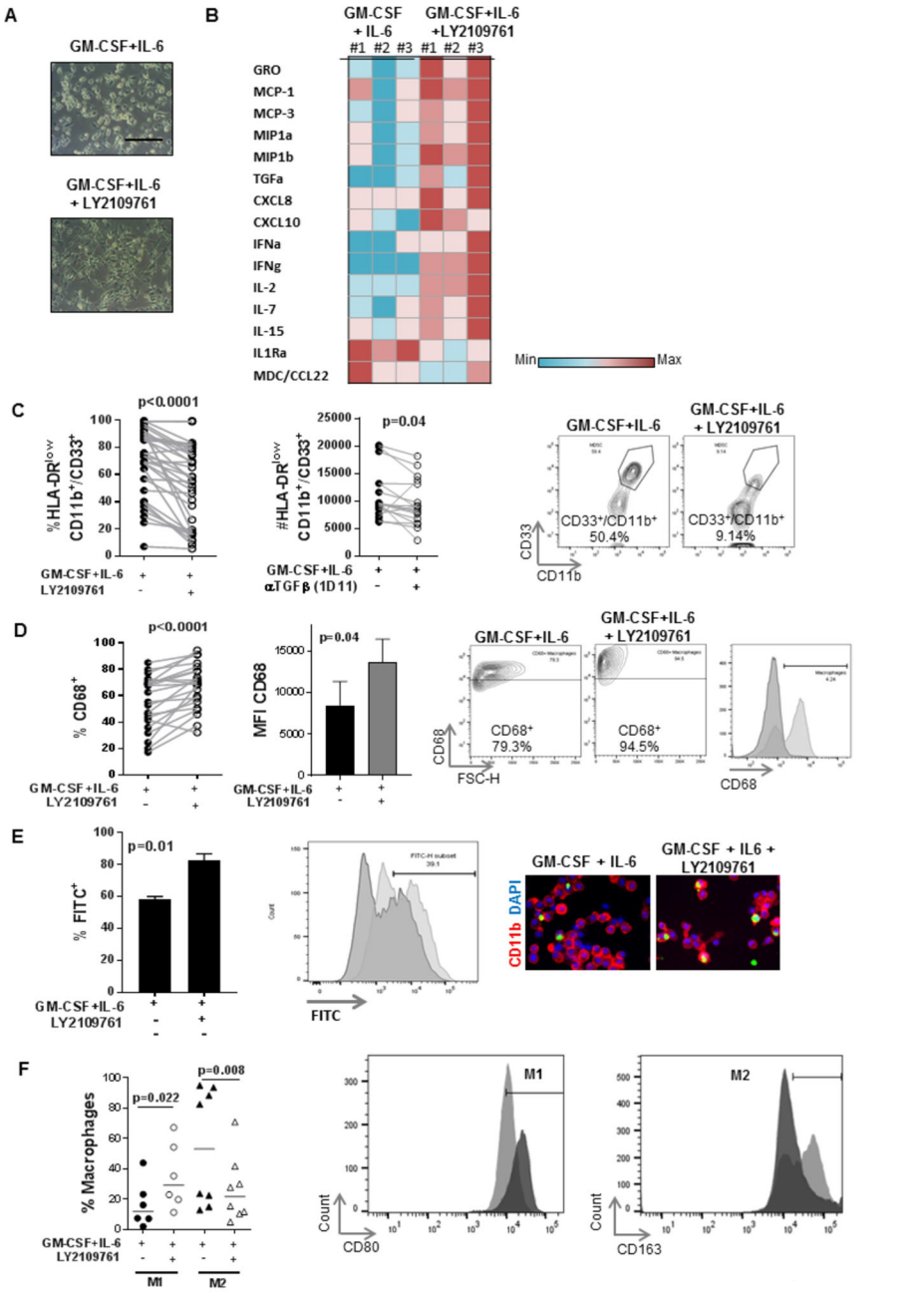

Fig. 6. Inhibition of TGFβ signaling alters differentiation of myeloid cells, reducing MDSCs and increasing secretion of pro-inflammatory molecules.

A. Representative bright field images of $CD14^+$ cultures with GM-CSF+IL6 and with the addition of TβRI inhibitor showing the different morphology of the cells after treatment. **B.** Quantification of pro-inflammatory cytokines and chemokines measured in the supernatants of $CD14^+$ cells cultured with GM-CSF+IL6 with the addition of TβRI inhibitor, LY2108761 (N=3). Normalized protein concentration is shown in Supplementary Fig. S7. **C.** Percentage of HLA-$DR^{low}CD11b^+CD33^+$ cells within the $CD14^+$ fraction after 5 days of treatment with GM-CSF and IL6 in combination with TβRI inhibitor (N=35) or with 1D11 (N=17). Representative FACS plots showing $CD11b^+/CD33^+$ cells within the $CD14^+$ /HLA-DR^{low}

population are shown in the right panels. **D.** Percentage of $CD68^+$ macrophages and MFI of CD68 measured by FACS after 5 days of treatment with GM-CSF and IL6 in combination with LY2108761 (N=8). Representative FACS plots of $CD68^+$ macrophages are shown on the right panels. Histogram representing CD68 fluorescence intensity (dark grey=GM-CSF +IL6, light grey=GM-CSF+IL6+LY2109761). **E.** Percentage of $FITC^+$ cells within the $CD11b^+$ population (N=3). Representative histogram for the FITC fluorescence on $CD11b^+$ cells treated with GM-CSF and IL6 (dark grey) and with the addition of LY2109761 (light grey). Representative immunofluorescence images are shown in the right. $CD11b^+$ cells are shown in red, $FITC^+$ beads are shown in green. **F.** Percentage $CD80^+$ M1 and $CD163^+$ M2 macrophages within the $CD68^+$ macrophage population generated after 5 days of treatment as in A (N=6). Representative overlay graphs are shown in the right (light grey= GM-CSF +IL6, dark grey=GM-CSF+IL6+LY2109761).

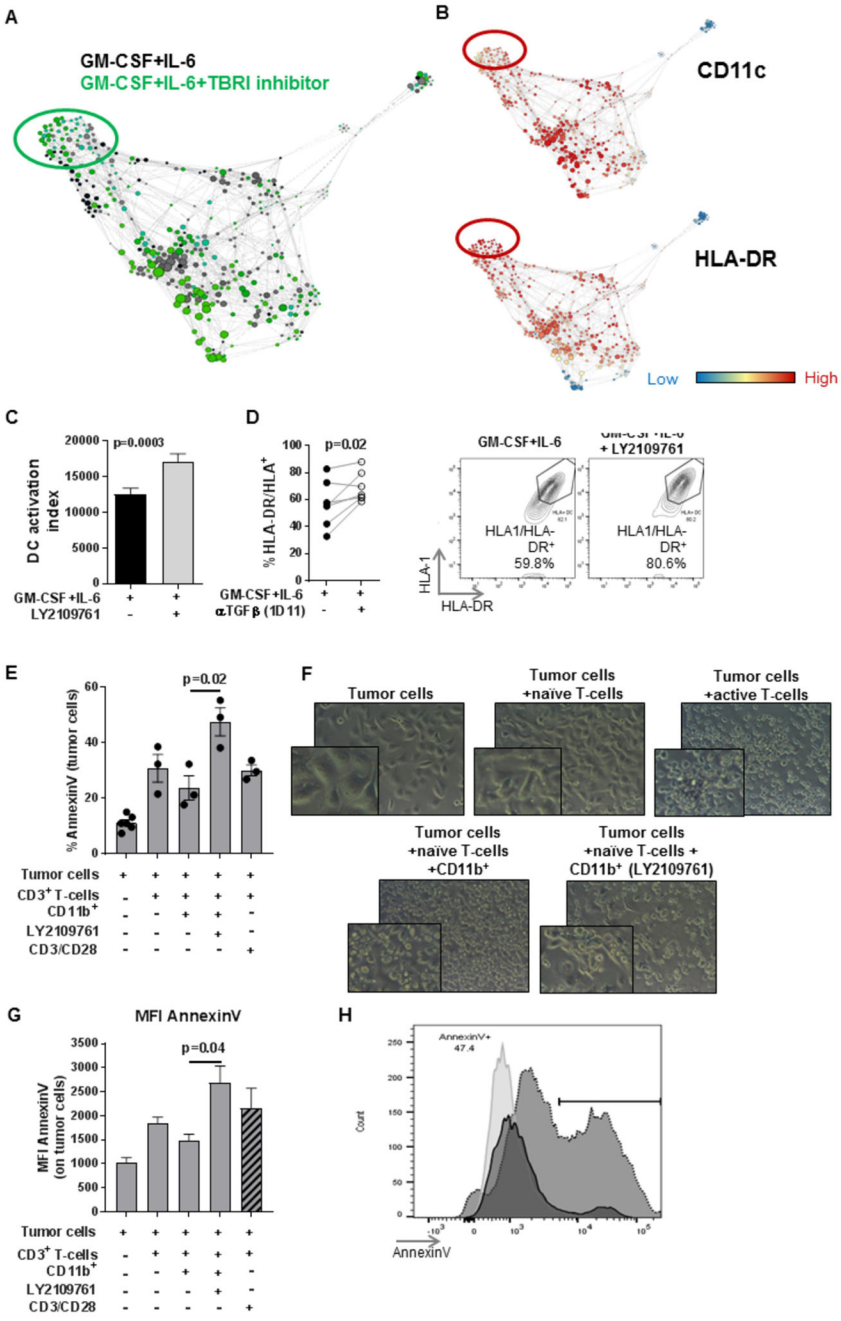

Fig. 7. Inhibition of TGFβ promotes mature antigen-presenting dendritic cells.

A. CyTOF force-directed scaffold map of GM-CSF+IL6 treated cells (grey) and with the addition of LY2109781 (green) (N=4). **B.** Relative abundance of surface markers CD11c and HLA-DR on the previous populations. **C**. DC activation was measured by quantification of Median Fluorescence Intensity of DC activation markers: HLA1, HLA-DR, CD86, CD11c and CD40 on samples treated as in A-B (N=9). **D**. Similar results were obtained when cells were treated with 1D11 to inhibit TGFβ (N=6). Representative FACS plots showing the percentage of mature antigen-presenting DC ($HLA1^+$/$HLA\text{-}DR^+$). **E**. Quantification of tumor cell killing in co-cultures of human tumor cells (H1299), myeloid cells, and

autologous naïve T-cells as described in Supplementary Fig. S7. Percentage of annexinV^+ on CD45-negative tumor cells. T cells activated with CD3/CD28 beads were used as a positive control (N=5). **F.** Representative bright field images of myeloid cells, T-cells and tumor cells co-cultures. **G.** AnnexinV^+ MFI on tumor cells after co-culture with myeloid cells and autologous naïve $CD3^+$ T cells. **H.** Representative histogram of annexinV fluorescence intensity. Light gray: tumor cells were co-cultured with $CD3^+$ T cells and $CD11b^+$ myeloid cells that were generated under TGFβ inhibition (LY2109761); dark grey: tumor cells after co-culture with T cells and $CD11b^+$ cells that were generated with cytokines GM-CSF and IL6 alone.